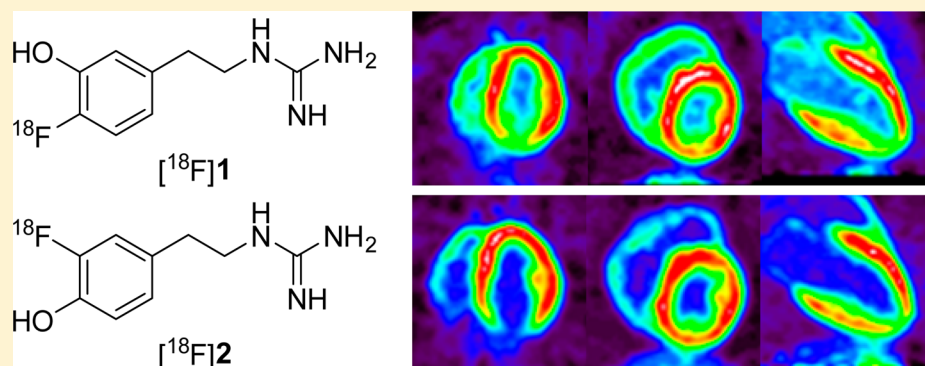


[¹⁸F]Fluoro-Hydroxyphenethylguanidines: Efficient Synthesis and Comparison of Two Structural Isomers as Radiotracers of Cardiac Sympathetic Innervation

Yong-Woon Jung, Keun Sam Jang, Guie Gu, Robert A. Koeppe, Phillip S. Sherman, Carole A. Quesada, and David M. Raffel*

Division of Nuclear Medicine, Department of Radiology, 2276 Medical Sciences I Building, University of Michigan Medical School, Ann Arbor, Michigan 48109, United States



ABSTRACT: Fluorine-18 labeled phenethylguanidines are currently under development in our laboratory as radiotracers for quantifying regional cardiac sympathetic nerve density using PET imaging techniques. In this study, we report an efficient synthesis of ¹⁸F-hydroxyphenethylguanidines consisting of nucleophilic aromatic [¹⁸F]fluorination of a protected diaryliodonium salt precursor followed by a single deprotection step to afford the desired radiolabeled compound. This approach has been shown to reliably produce 4-[¹⁸F]fluoro-*m*-hydroxyphenethylguanidine ([¹⁸F]4F-MHPG, [¹⁸F]1) and its structural isomer 3-[¹⁸F]fluoro-*p*-hydroxyphenethylguanidine ([¹⁸F]3F-PHPG, [¹⁸F]2) with good radiochemical yields. Preclinical evaluations of [¹⁸F]2 in nonhuman primates were performed to compare its imaging properties, metabolism, and myocardial kinetics with those obtained previously with [¹⁸F]1. The results of these studies have demonstrated that [¹⁸F]2 exhibits imaging properties comparable to those of [¹⁸F]1. Myocardial tracer kinetic analysis of each tracer provides quantitative metrics of cardiac sympathetic nerve density. Based on these findings, first-in-human PET studies with [¹⁸F]1 and [¹⁸F]2 are currently in progress to assess their ability to accurately measure regional cardiac sympathetic denervation in patients with heart disease, with the ultimate goal of selecting a lead compound for further clinical development.

KEYWORDS: 3-[¹⁸F]Fluoro-*p*-hydroxyphenethylguanidine, [¹⁸F]3F-PHPG, 4-[¹⁸F]fluoro-*m*-hydroxyphenethylguanidine, [¹⁸F]4F-MHPG, norepinephrine transporter, sympathetic nervous system

INTRODUCTION

Cardiac autonomic dysfunction contributes to morbidity and mortality in many diseases that damage the heart, including congestive heart failure, myocardial ischemia, myocardial infarction, and diabetic autonomic neuropathy.^{1–3} Disease-induced alterations in the nervous control of the heart can be caused by changes in the outflow of nervous impulses to the parasympathetic and sympathetic branches of the autonomic nervous system arising from central sites in the brain, and by regional degeneration of postganglionic parasympathetic and/or sympathetic nerve fibers in the heart. The complex interaction between aberrant parasympathetic and sympathetic influences on the heart often evolves with the progression of disease. For example, early heart failure is characterized by hyperactivity of sympathetic nerve pathways, with a concomitant reduction in parasympathetic activation, a process that

referred to as “parasympathetic withdrawal”.⁴ The chronically elevated levels of the neurotransmitter norepinephrine that result from this imbalance of parasympathetic and sympathetic influences are cardiotoxic and contribute to the progression of heart failure, including development of left ventricular dilation.^{5,6} Throughout the time course of heart failure, autonomic dysfunction can promote malignant arrhythmias, leading to sudden cardiac death.^{7,8}

Clinical imaging studies of cardiac sympathetic denervation using nuclear scintigraphy techniques have provided important insights into how different diseases affect this nerve population.^{9,10} Our laboratory has previously developed several

Received: February 1, 2017

Accepted: March 21, 2017

Published: March 21, 2017

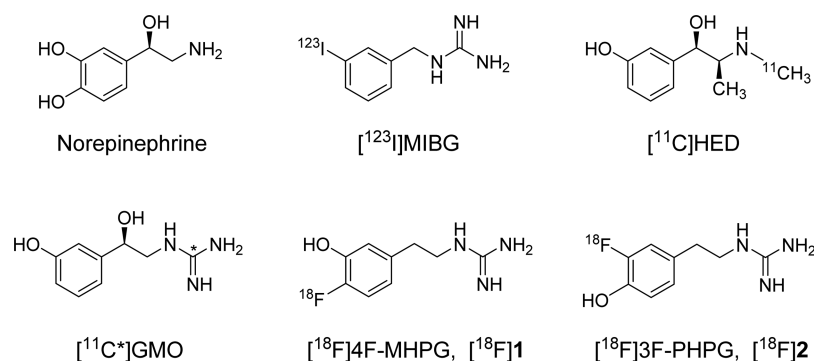


Figure 1. Structures of norepinephrine and some radiotracers for imaging cardiac sympathetic nerve terminals.

radiotracers for noninvasive imaging studies of cardiac sympathetic nerves, including [¹²³I]metaiodobenzylguanidine ([¹²³I]MIBG) for planar scintigraphy and SPECT imaging, and [¹¹C]-(-)-*m*-hydroxyephedrine ([¹¹C]HED) for PET imaging (Figure 1).^{11,12} These radiolabeled analogs of the endogenous neurotransmitter norepinephrine are transported into presynaptic sympathetic nerve terminals by the norepinephrine transporter (NET). Since NET expression in the heart is only associated with sympathetic nerve varicosities, the cardiac retention levels of these tracers can be used as metrics of regional sympathetic nerve density. Clinical trials with [¹²³I]MIBG and [¹¹C]HED tracers in heart failure patients have demonstrated that cardiac sympathetic denervation is associated with a significantly increased risk of sudden cardiac death. For example, the multicenter ADMIRE-HF study of 961 heart failure patients showed that a low heart-to-mediastinum ratio (H/M) of [¹²³I]MIBG obtained from planar gamma camera images, a global measure of cardiac sympathetic denervation, was a predictor of mortality and fatal arrhythmic events in patients eligible for implantable cardioverter defibrillator (ICD) therapy.¹³ More recently, the prospective PAREPET trial used [¹¹C]HED to assess regional sympathetic denervation, [¹³N]ammonia to assess myocardial perfusion, and [¹⁸F]FDG to assess myocardial viability in 204 heart failure patients staged for an ICD.¹⁴ The PAREPET results showed that the regional extent of sympathetic denervation in the left ventricle (as defined by [¹¹C]HED retention deficits) was the strongest predictor of sudden cardiac arrest among all imaging parameters measured. Patients with regional sympathetic denervation encompassing more than 38% of their left ventricle defined the upper tertile of patients with the highest risk of sudden cardiac arrest ($p < 0.001$). The results of the ADMIRE-HF and PAREPET trials suggest that noninvasive imaging studies of cardiac sympathetic denervation may find a clinical role in improved risk stratification of heart failure patients for ICD placement.¹⁵

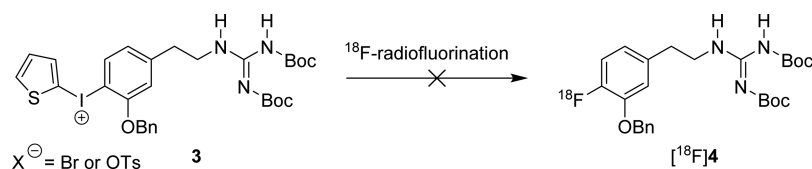
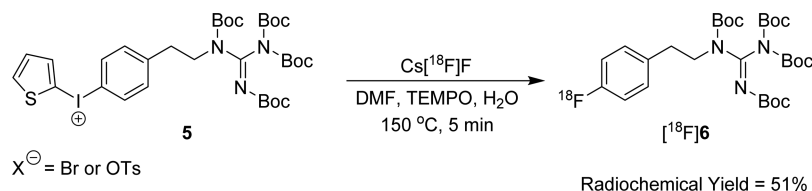
We have recently been investigating radiolabeled phenethylguanidines as next generation sympathetic nerve tracers with improved myocardial kinetics for accurate and sensitive quantification of regional sympathetic nerve density using PET and tracer kinetic analysis methods.¹⁶ Our initial work focused on the carbon-11 labeled hydroxyphenethylguanidine *N*-[¹¹C]guanyl-(-)-*m*-octopamine ([¹¹C]GMO, Figure 1). PET studies with [¹¹C]GMO in nonhuman primates showed that the myocardial kinetics of this tracer could be successfully analyzed using compartmental modeling methods or Patlak graphical analysis to obtain an estimates of the “net uptake rate constant” K_i (mL/min/g) as a measure of regional sympathetic

nerve density.¹⁷ In control studies and pharmacological blocking studies with the NET inhibitor desipramine (DMI) in rhesus macaque monkeys, the K_i values from compartmental modeling analysis were found to decrease with increasing DMI doses along a sigmoidal dose–response curve, with an IC_{50} of 0.087 mg/kg and a Hill slope $n_H = -0.70$. Similar results were obtained using the Patlak slopes K_p (mL/min/g) from Patlak graphical analysis of [¹¹C]GMO kinetics, as an alternative estimate of the K_i values ($IC_{50} = 0.068$ mg/kg, $n_H = -0.54$). These results strongly suggest that regional estimates of K_i from tracer kinetic analysis of [¹¹C]GMO kinetics in human hearts would serve as a reproducible metric of regional cardiac sympathetic nerve density.

While the preclinical PET studies with [¹¹C]GMO were highly encouraging, the short half-life of carbon-11 (20.4 min) limits its use to PET centers with an on-site cyclotron. Conversely, fluorine-18 has a sufficiently long half-life (1.83 h) that the production and distribution of ¹⁸F-labeled radiopharmaceuticals from a central production facility to stand-alone PET imaging centers is feasible. To develop a fluorine-18 labeled phenethylguanidine, we initially chose to prepare 4-[¹⁸F]fluoro-*m*-hydroxyphenethylguanidine ([¹⁸F]4F-MHPG, [¹⁸F]1, Figure 1). In previous studies in an isolated rat heart model, the kinetics of [¹¹C]4F-MHPG were comparable to those of [¹¹C]GMO.¹⁶

A previous report described several preclinical evaluations of [¹⁸F]1, including PET imaging studies in nonhuman primates.¹⁸ The results of the PET studies of [¹⁸F]1 closely paralleled those obtained with [¹¹C]GMO,¹⁷ supporting further development of this agent for clinical translation. For these pilot studies, our initial approach to the preparation of [¹⁸F]1 was a multistep automated radiosynthesis involving production of a ¹⁸F-labeled intermediate using a diaryliodonium salt precursor followed by a deprotection step, an *N*-guanylation step, a second deprotection step and finally HPLC purification to provide [¹⁸F]1.¹⁸ Because of the multiple steps required, this initial method relied on the use of two automated radiosynthesis modules in adjacent hot-cells, linked in series, to provide the final product. While this approach was adequate for preclinical evaluations of [¹⁸F]1, it was poorly suited to routine production of the radiotracer for clinical studies in human subjects. Thus, one goal of this work was to develop an efficient automated radiosynthesis of [¹⁸F]1 capable of providing sufficiently high radiochemical yields for clinical PET studies.

We report here a new two-step approach to the radiosynthesis of [¹⁸F]1 that utilizes a novel *N,N',N'',N'''*-tetrakis-Boc protected guanidinyliodonium salt precursor for nucleophilic aromatic [¹⁸F]fluorination, followed by a single deprotection

Scheme 1. Ineffective Initial Approach to an Improved Radiosynthesis of [^{18}F]1Scheme 2. ^{18}F -Fluorination of a Test Compound with a Fully Protected Guanidinylium MoietyTable 1. [^{18}F]Fluorination of Diaryliodonium Salts (**5**, **11** and **21**) under Various Conditions

entry	I ⁺ salt ^a	^{18}F -fluoride [^{18}F]F [−] X ⁺	method	T (°C)	t (min)	solvent ^b	TEMPO and H ₂ O ^b	product	yield (%) ^c	n
1	5	[^{18}F]F [−] K ⁺	manual	150	10	MeCN	—	[^{18}F]6	NR	2
2	5	[^{18}F]F [−] K ⁺	manual	150	10	DMF	—	[^{18}F]6	3 ± 2	2
3	5	[^{18}F]F [−] TBA ⁺	manual	150	10	DMF	—	[^{18}F]6	trace	2
4	5	[^{18}F]F [−] Cs ⁺	manual	150	10	DMF	—	[^{18}F]6	9 ± 2	2
5	5	[^{18}F]F [−] Cs ⁺	manual	150	5	DMF	+	[^{18}F]6	51 ± 5	3
6	5	[^{18}F]F [−] Cs ⁺	manual	130	5	DMF	+	[^{18}F]6	31 ± 5	3
7	5	[^{18}F]F [−] Cs ⁺	manual	120	5	DMF	+	[^{18}F]6	28 ± 3	3
8	5	[^{18}F]F [−] Cs ⁺	manual	150	15	DMF	+	[^{18}F]6	43 ± 5	2
9	5	[^{18}F]F [−] Cs ⁺	manual	150	25	DMF	+	[^{18}F]6	30 ± 5	2
10	11	[^{18}F]F [−] Cs ⁺	manual	150	5	DMF	+	[^{18}F]22	16 ± 5	5
11	11	[^{18}F]F [−] Cs ⁺	manual	150	15	DMF	+	[^{18}F]22	11 ± 4	3
12	11	[^{18}F]F [−] Cs ⁺	automated	150	5	DMF	+	[^{18}F]1	7.0 ± 3.5 ^d	13
13	21	[^{18}F]F [−] Cs ⁺	automated	150	5	DMF	+	[^{18}F]2	8.0 ± 3.5 ^e	12

^aAmount of diaryliodonium salt precursor used was 4–6 mg. ^bReaction solvent (MeCN or DMF; 500 μL) prepared without (—) or with (+) 1 mg TEMPO and 10 μL of H₂O. ^cProgress of the reaction and yields for manual reactions were analyzed by radio-TLC (developing solvent: ethyl acetate/hexane = 30:70, vol/vol). ^dYield of the isolated pure product [^{18}F]1 by semipreparative column (Phenomenex Synergi 10 μ Hydro-RP 80A, 250 \times 10 mm) using HPLC (5% EtOH in 40 mM NH₄OAc buffer, λ = 254 nm, 4.0 mL/min). ^eYield of the isolated pure product [^{18}F]2 by semipreparative column (Phenomenex Synergi 10 μ Hydro-RP 80A, 250 \times 10 mm) using HPLC (3.5% EtOH in 40 mM NH₄OAc buffer, λ = 254 nm, 4.0 mL/min).

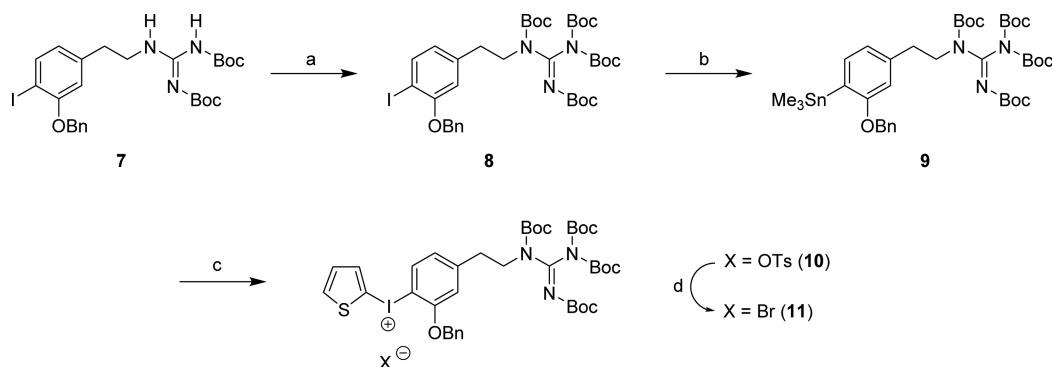
step, to provide [^{18}F]1 in good yields and high specific activities for clinical PET studies. This new approach is performed using a single automated radiosynthesis module and has proven to be very reliable.

With the establishment of this new synthetic approach to ^{18}F -hydroxyphenethylguanidines, the second objective of this study was to prepare 3- ^{18}F fluoro-*p*-hydroxyphenethylguanidine ([^{18}F]3F-PHPG, [^{18}F]2, Figure 1), the structural isomer of [^{18}F]1. Preclinical evaluations of this compound were performed to compare its characteristics as a cardiac innervation tracer with those of [^{18}F]1. Studies in nonhuman primates showed that [^{18}F]2 is as good or better than [^{18}F]1 as a cardiac PET imaging agent. Based on the positive preclinical testing results with [^{18}F]1 and [^{18}F]2, these new cardiac sympathetic innervation radiotracers are currently being evaluated in first-in-human PET studies under an exploratory investigational new drug (IND) clearance from the FDA.

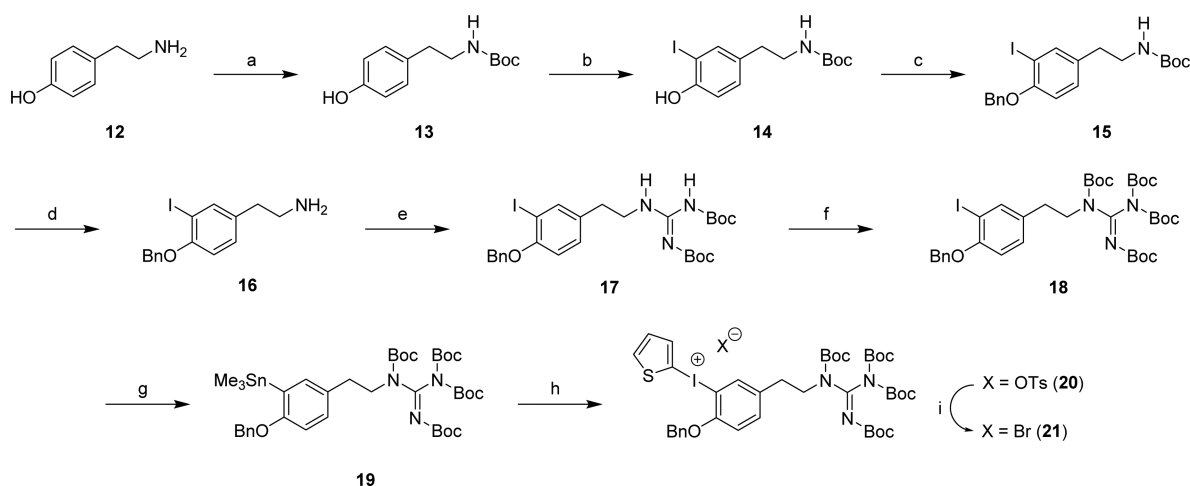
RESULTS AND DISCUSSION

Chemistry and Radiochemistry. Our initial strategy for improving the radiosynthesis of [^{18}F]1 was to utilize a *N,N'*-bis-Boc-protected diaryliodonium salt precursor for direct no-carrier-added nucleophilic aromatic [^{18}F]fluorination via a two-

step automated radiosynthesis (Scheme 1). However, many attempts at ^{18}F -radiofluorination of the *N,N'*-bis-Boc-guanidinyliodonium salt precursor **3** with different [^{18}F]fluoride sources under a variety of reaction conditions were unsuccessful in providing the desired ^{18}F -labeled intermediate [^{18}F]4. We hypothesized that this disappointing outcome was related to the two unprotected protons of the guanidinylium group being acidic, causing a disturbance in the ^{18}F -radiofluorination reaction. To confirm this hypothesis, we explored the ^{18}F -radiofluorination of a test compound with a fully protected guanidinylium moiety to eliminate the unprotected protons (Scheme 2). The *N,N',N'',N'''*-tetrakis-Boc-guanidinyliodonium salt precursor **5** was synthesized, and radiolabeling tests were carried out under various conditions, including different [^{18}F]fluoride sources, reaction solvents (e.g., DMF and MeCN), reaction times and reaction temperatures to produce the ^{18}F -labeled compound [^{18}F]6 (Table 1).¹⁹ The reaction of K[^{18}F]F–K₂₂₂ or [^{18}F]TBAF with precursor **5** afforded [^{18}F]6 in low yields (0–3%) at 150 °C for 10 min. When precursor **5** was reacted with Cs[^{18}F]F under general anhydrous radiofluorination conditions, the yield of [^{18}F]6 was improved (~9% at 150 °C for 10 min). However, when **5** was reacted with Cs[^{18}F]F for a longer reaction time (150 °C for 25 min), the yield of the

Scheme 3. Synthetic Route to the Diaryliodonium Salt Precursor 11^a

^a(a) (Boc)₂CO, DMAP, Et₃N, THF, rt, 48h, 92%; (b) Sn₂Me₆, Pd(PPh₃)₄, toluene, reflux, N₂, 30 min, 86%; (c) (i) 2-(diacetoxyiodo)thiophene, *p*-TsOH·H₂O, MeCN, CH₂Cl₂, N₂, rt, 1 h; (ii) 9, MeCN, CH₂Cl₂, N₂, rt, 20 h, 87%; (d) KBr, MeCN, H₂O, 65 °C-rt, 1 h, 86%.

Scheme 4. Synthetic Route to the Diaryliodonium Salt Precursor 21^a

^a(a) (Boc)₂CO, Et₃N, THF, rt, 24 h, 98%; (b) NaI, NaOCl, KOH, MeOH, 0 °C, 43%; (c) BnBr, K₂CO₃, acetone, 4 h, 78%; (d) HCl, 65 °C, 1 h, 97%; (e) 1,3-*N,N'*-bis(*tert*-butoxycarbonyl)-2-methyl-2-thiopseudourea, Et₃N, DMF, 0 °C-rt, 24 h, 58%; (f) (Boc)₂CO, DMAP, Et₃N, THF, rt, 20 h, 63%; (g) Sn₂Me₆, Pd(PPh₃)₄, toluene, reflux, N₂, 30 min, 98%; (h) (i) 2-(diacetoxyiodo)thiophene, *p*-TsOH·H₂O, MeCN, CH₂Cl₂, N₂, rt, 1 h; (ii) 19, MeCN, CH₂Cl₂, N₂, rt, 44 h, 86%; (i) KBr, MeCN, H₂O, 65 °C to rt, 1 h, 96%.

desired product decreased to ~4%. We hypothesized that the reduced radiochemical yields at longer reaction times might be due to the decomposition of the iodonium salt precursor 5 and the radiofluorinated product [¹⁸F]6 at the 150 °C reaction temperature. In tests, 5 started slow thermal decomposition at 150 °C in open capillary tubes in a melting point apparatus, supporting this hypothesis. The addition of TEMPO (1.0 mg) as a radical scavenger and a small amount of water (10 μL) in the reaction solvent (DMF, 0.5 mL) to increase the solubility of Cs[¹⁸F]F greatly increased the radiochemical yields, up to ~51% for manual syntheses at 150 °C for 5 min. Additional tests using a reduced temperature of 130 °C for 5 min, decreased the yield of [¹⁸F]6 to ~31%. Tests at temperatures greater than 150 °C did not produce any improvements in the yields.

This encouraging result led us to prepare the required *N,N',N'',N'''*-tetrakis-Boc-protected guanidinyliodonium salt precursor for a simplified automated production of [¹⁸F]1 for clinical studies (Scheme 3). The *N,N'*-bis-Boc-protected iodophenethylguanidine 7 was previously synthesized in our laboratory.¹⁸ This compound was converted to the *N,N',N'',N'''*-tetrakis-Boc-protected guanidine 8 by treatment

with di-*t*-butyl dicarbonate in the presence of dimethylamino-pyridine and triethylamine in THF. Reaction of 8 with bis(trimethyl)tin in the presence of tetrakis(triphenylphosphine)palladium provided the trimethylstannane compound 9. [2-hydroxy(tosyloxy)iodo]thiophene,²⁰ which was generated in situ by a mixture of 2-(diacetoxyiodo)-thiophene²¹ with *p*-toluenesulfonic acid under nitrogen atmosphere, was reacted with trimethylstannane 9 to provide (2-thienyl)iodonium tosylate 10 in 87% yield as a yellow solid. Among various counteranions, bromide was found to be especially reactive, increasing the radiochemical yield.²² Therefore, (2-thienyl)iodonium tosylate 10 was converted into the corresponding bromide 11 as a gray powder in 86% yield using KBr in a solution of CH₃CN and H₂O.

A similar approach was used to prepare the guanidinyliodonium salt precursor 21 for production of [¹⁸F]2 (Scheme 4). The *N*-Boc-protected tyramine 13 was iodinated in the presence of sodium iodide and sodium hypochlorite to afford 14 in low yields (43%). The iodophenol 14 was protected by benzylation with benzyl bromide followed by subsequent deprotection of the Boc group to afford the benzylated 3-iodotyramine intermediate 16. Condensation of 16 with 1,3-

human imaging studies with [^{123}I]MIBG and [^{11}C]HED because the isolated rat heart has coronary flow rates that are about 10 times higher than resting blood flow in a human heart.²⁵ If tracer molecules diffuse out of sympathetic neurons in the isolated rat heart they are more likely to be cleared from interstitial spaces into the capillary bed rather than re-entering nerve terminals by NET transport. In contrast, several studies have shown that [^{11}C]HED continuously diffuses out of nerve terminals only to be taken back up into the nerves during PET studies in normal human hearts.^{25–27} The slower neuronal uptake rates and long neuronal retention times of [^{18}F]1 and [^{18}F]2 are favorable for tracer kinetic analysis,¹⁷ including Patlak graphical analysis, which requires irreversible trapping of a tracer in a tissue compartment.²⁸

PET Studies in Nonhuman Primates. Dynamic PET studies with [^{18}F]2 were performed in rhesus macaque monkeys to characterize the imaging properties, metabolism and myocardial kinetics of the tracer ($n = 4$). Representative cardiac PET images of [^{18}F]2 show that the tracer provides high quality images of the distribution of sympathetic nerve terminals in the heart (Figure 3). Corresponding PET images

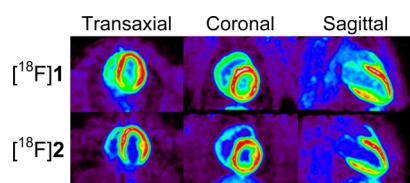


Figure 3. Representative PET images of [^{18}F]1 and [^{18}F]2 in rhesus macaque monkeys.

for [^{18}F]1 are also provided. There is little retention of either tracer in the lungs, providing very high heart-to-lung contrast. [^{18}F]2 exhibited good heart-to-blood (H/B) contrast in the final PET images ($t = 85$ min), with $\text{H/B} = 4.0 \pm 0.3$. This was better heart-to-blood contrast than the ratio measured for [^{18}F]1, which was $\text{H/B} = 3.0 \pm 0.5$.^{17,18} Final heart-to-liver (H/L) ratios for [^{18}F]2 were 2.2 ± 0.8 . Due to faster clearance of activity from the liver, contrast between heart and liver was a little better for [^{18}F]1, with final $\text{H/L} = 2.5 \pm 0.3$. No significant uptake of free fluorine-18 was observed in the vertebral bones of the spine for either compound, indicating that these tracers are not susceptible to defluorination in nonhuman primates.

Metabolism of [^{18}F]2. To assess the metabolism of [^{18}F]2, six venous blood samples were drawn during the dynamic PET studies. Plasma was separated from blood and processed for analysis on a reverse-phase HPLC system with an in-line radiation detector optimized for detection of 511 keV positron annihilation photons to determine the fraction of plasma activity in the form of radiolabeled metabolites.¹⁸ Representative data showing the metabolic breakdown of [^{18}F]2 in plasma are shown in Figure 4. Data on the metabolic breakdown of [^{18}F]1 in rhesus macaques are shown for comparison. For both compounds, the metabolism time course was biphasic, with an initially rapid phase of metabolism followed by a slower phase. [^{18}F]2 was metabolized more slowly than [^{18}F]1. The mean time at which 50% of parent radiotracer was still intact was 6.7 ± 2.4 min for [^{18}F]2 vs 2.3 ± 0.9 min for [^{18}F]1 ($n = 4$ each).

Using *in vitro* incubations of [^{18}F]1 with a monkey liver cytosol fraction and the cofactor for sulfur conjugation, 3'-phospho-adenosine-5'-phosphosulfate (PAPS), we previously

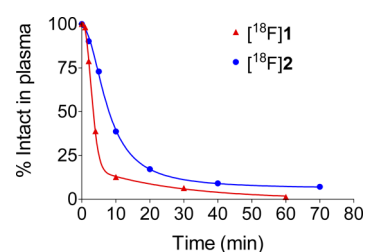


Figure 4. Time course of the metabolic breakdown of [^{18}F]1 and [^{18}F]2 in the plasma of rhesus macaque monkeys.

showed that the main metabolic pathway for this compound in rhesus macaques was sulfate conjugation at its *m*-hydroxyl group.¹⁸ Incubations of [^{18}F]2 under identical conditions were unable to produce any radiometabolite, suggesting that this compound is not a substrate for sulfate conjugation in rhesus monkeys. Additional *in vitro* tests with [^{18}F]2 using a monkey liver microsomal fraction and the glucuronidation cofactor uridine 5'-diphospho-glucuronic acid (UDPGA) were also negative. Further tests are needed to identify the unknown polar metabolite of [^{18}F]2 produced in rhesus macaque monkeys.

Blood Activity Partitioning. Using aliquots of plasma and whole blood, the ratio of the activity concentration in plasma (C_p) over that in whole blood (C_{wb}) was determined for each venous blood sample. For [^{18}F]2, the mean ratio C_p/C_{wb} measured was 1.23 ± 0.05 ($n = 4$). The C_p/C_{wb} ratio tended to be constant throughout the PET study. This is similar to previous results for [^{18}F]1 which found $C_p/C_{wb} = 1.25 \pm 0.06$ ($n = 4$).¹⁸

Tracer Kinetic Analysis. The myocardial tissue kinetics $C_t(t)$ of [^{18}F]2 and its estimated kinetics in plasma $C_p(t)$ were analyzed using compartmental modeling and Patlak graphical analysis as previously described.^{17,18} For compartmental modeling analysis, the model used has two tissue compartments, one for extraction into and clearance from extracellular spaces, with rate constants K_1 (mL/min/g) and k_2 (min^{-1}), respectively, and the second for irreversible uptake into sympathetic neurons, with rate constant k_3 (min^{-1}). A blood volume fraction term BV (dimensionless) was also included to account for activity in myocardial blood. The estimates of K_1 , k_2 , and k_3 from compartmental modeling were used to calculate a "net uptake rate constant" K_i (mL/min/g) = $(K_1 k_3)/(k_2 + k_3)$, which reflects the net rate of tracer influx into tissue compartments. K_1 estimates were fairly consistent for [^{18}F]2, while k_2 and k_3 were more variable, similar to previous findings with [^{18}F]1. The mean values of K_1 for [^{18}F]2 were $K_1 = 0.46 \pm 0.05$ mL/min/g, compared with $K_1 = 0.56 \pm 0.07$ mL/min/g for [^{18}F]1. Estimates of k_3 (the rate constant related to neuronal uptake of the tracer) were too variable to be useful as a quantitative measure of nerve density, but the values of the net uptake rate constant K_i calculated from the rate constant estimates were very consistent. For [^{18}F]2, the mean net uptake rate constant was $K_i = 0.221 \pm 0.029$ mL/min/g, which can be compared with $K_i = 0.341 \pm 0.041$ mL/min/g for [^{18}F]1. Patlak graphical analysis also gave consistent results. This analysis approach uses a mathematical transformation of $C_p(t)$ and $C_t(t)$ to construct a "Patlak plot" which has a distinct linear phase. The slope of the linear phase, the Patlak slope K_p (mL/min/g), is theoretically equal to the calculated net uptake rate constant K_i derived from the compartmental modeling rate constants. For [^{18}F]2, the measured Patlak slopes averaged $K_p = 0.169 \pm$

0.021 mL/min/g, compared with $K_p = 0.302 \pm 0.031$ mL/min/g for [^{18}F]1. For any given study, relative to their corresponding K_i values, the Patlak slopes are biased a little lower in magnitude because Patlak analysis does not account for myocardial blood activity in the tissue kinetics $C_t(t)$, while the blood volume term BV used in compartmental modeling does account for the blood activity. Representative examples of the results of compartmental modeling and Patlak analysis of [^{18}F]2 are shown in Figure 5. In previous PET studies in

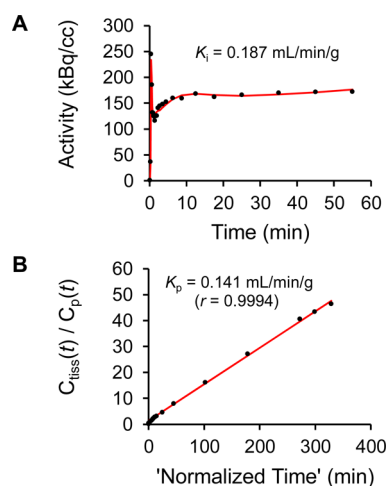


Figure 5. Myocardial tracer kinetic analyses for [^{18}F]2 kinetics in the same monkey. Parameter estimates from compartment modeling (A) were used to calculate a net uptake rate constant K_i (mL/min/g). Patlak graphical analysis (B) provided a Patlak slopes K_p (mL/min/g).

nonhuman primates with [^{11}C]GMO and [^{18}F]1, using the NET inhibitor desipramine (DMI) to pharmacologically induce different degrees of NET transporter occlusion showed that net uptake rate constants K_i and Patlak slopes K_p each tracked sensitively and reproducibly with DMI-induced declines in available NET transporters.^{17,18} Taken together, the results of these studies suggest that values of K_i or K_p obtained from tracer kinetic analysis of the kinetics of [^{18}F]1 or [^{18}F]2 can be used as quantitative metrics of regional sympathetic nerve density in the heart.

Advantages of ^{18}F -Hydroxyphenethylguanidines.

[^{18}F]1 and [^{18}F]2 offer some advantages over existing cardiac sympathetic innervation radiotracers. The longer half-life of a fluorine-18 (1.83 h) compared with the 20.4 min half-life of carbon-11 in compounds such as [^{11}C]HED and [^{11}C]GMO was one advantage discussed previously. In terms of structure–activity relationships, there are four major factors that govern the neuronal uptake and retention kinetics of sympathetic nerve radiotracers: (a) rate of neuronal uptake by NET (equal to V_{\max}/K_m for NET transport); (b) rate of vesicular uptake (equal to V_{\max}/K_m for VMAT2 transport); (c) vulnerability to intraneuronal metabolism by enzymes such as monoamine oxidase (MAO); and (d) membrane diffusion rates, which influence vesicular storage and neuronal retention, and are partly determined by a tracer's lipophilicity ($\log P$). [^{18}F]1 and [^{18}F]2 were developed in an effort to design a tracer with optimal properties in each of these four categories. We hypothesized that such a tracer would possess myocardial kinetics that could be successfully analyzed using established tracer kinetic analysis techniques to provide quantitative measures of regional sympathetic nerve density. Specifically,

the targeted properties were (a) slower NET transport rates than [^{11}C]HED and [^{123}I]MIBG; (b) rapid vesicular uptake due to efficient VMAT2 transport; (c) resistance to intraneuronal metabolism; and (d) low lipophilicity to promote long neuronal retention times. The slower neuronal uptake rate makes the rate constant associated with this process more identifiable from the cardiac PET kinetics, and the rapid uptake and long retention in storage vesicles eliminates one rate constant from the kinetic model, leading to more reliable and consistent parameter estimates.¹⁷

To achieve this goal, radiolabeled phenethylguanidines were investigated because several phenethylguanidines are potent neuron blocking agents due to their prolonged retention inside norepinephrine storage vesicles.^{29–31} The isolated rat heart studies with [^{18}F]1 and [^{18}F]2 presented above (Figure 2) demonstrate that these compounds satisfy the targeted properties (a), (b), and (d). PET studies showing very long neuronal retention times for [^{18}F]1 and [^{18}F]2 in nonhuman primate myocardium are consistent with (b) rapid vesicular uptake and (d) very little diffusion of the tracers from storage vesicles. For (c), the guanidine group of the side chain of [^{18}F]1 and [^{18}F]2 confers stability against neuronal enzymes such as tyrosine hydroxylase, MAO, dopamine- β -hydroxylase, or DOPA decarboxylase.³² Previous studies with the carbon-11 analog of [^{18}F]1 in rats showed that 100% of the activity in the myocardium at $t = 30$ min after tracer administration was in the form of the parent tracer, consistent with no intraneuronal metabolism of the tracer.³³ Thus, [^{18}F]1 and [^{18}F]2 have been found to satisfy all of our targeted neuronal tracer properties.

Structure–activity studies of a series of ^{11}C -labeled phenethylguanidines in the isolated rat heart showed that several hydroxyphenethylguanidines had extremely long retention times in this model. This was particularly true for ring hydroxylation at the *m*- and *p*- positions, the *beta*-position of the side chain, or combinations of these hydroxyl substitutions.¹⁶ In contrast, none of the ^{11}C -labeled benzylguanidine compounds tested, including [^{11}C]-*p*-hydroxybenzylguanidine, were found to have long neuronal retention times in the isolated rat heart. These results suggest that hydroxyphenethylguanidines are better VMAT2 substrates than benzylguanidines, or are retained in storage vesicles much more efficiently, leading to high uptake and prolonged retention in storage vesicles. The highly acidic interior of vesicles has been described as an “amine trap”, since the low pH inside vesicles further encourages high pK_a molecules to exist in their ionized form.³⁴ The very high pK_a of the guanidine group of hydroxyphenethylguanidines ($pK_a = 10$ to 13) likely causes them to be highly protonated inside vesicles, further enhancing their vesicular retention.

Two ^{18}F -labeled analogs of [^{123}I]MIBG, *m*-[^{18}F]-fluorobenzylguanidine ([^{18}F]MFBG) and *p*-[^{18}F]-fluorobenzylguanidine ([^{18}F]PFBG) were synthesized previously for PET studies of cardiac sympathetic innervation and neuroendocrine tumors.^{35,36} Studies of [^{18}F]PFBG in the isolated rat heart model showed it had a neuronal uptake rate $K_{up} = 2.80$ mL/min/g wet, $\sim 77\%$ of the rate of 3.65 mL/min/g wet measured for [^{123}I]MIBG.^{16,37} The major neuronal clearance half-time for [^{18}F]PFBG was $T_{1/2} = 0.59$ h, compared with $T_{1/2} = 2.1$ h for [^{123}I]MIBG. Thus, [^{18}F]PFBG has rapid NET transport rate into sympathetic neurons and clears from the neurons faster than [^{123}I]MIBG. We are not aware of any human cardiac imaging studies with [^{18}F]PFBG or [^{18}F]MFBG, although one report used [^{18}F]PFBG to assess cardiac nerve

damage in a canine model of infarction.³⁸ While these tracers are certainly capable of imaging cardiac sympathetic nerves, their kinetics would not satisfy the four tracer properties we had targeted in the development of [¹⁸F]1 and [¹⁸F]2. Thus, another advantage of the ¹⁸F-hydroxyphenethylguanidines [¹⁸F]1 and [¹⁸F]2 over radiolabeled benzylguanidines is the ability to analyze their irreversible myocardial kinetics using standard tracer kinetic methods, such as Patlak analysis, to obtain quantitative regional estimates of sympathetic nerve density.

CONCLUSION

Our previous multistep radiosynthesis of [¹⁸F]1 was not a practical approach for routine production of [¹⁸F]fluoro-hydroxyphenethylguanidines in a clinical PET radiochemistry facility. A more efficient method involving ¹⁸F-labeling of a *N,N',N'',N'''*-tetrakis-Boc protected guanidinyliodoium salt precursor followed by a single deprotection step and HPLC purification has been developed. This new radiosynthetic approach has proven to be very reliable and provides sufficient radiochemical yields and specific activities for clinical studies in human subjects. This new method was used to synthesize [¹⁸F]2, a structural isomer of [¹⁸F]1. Preclinical tests of [¹⁸F]2 demonstrated that it has imaging properties and kinetics that are very similar to those observed with [¹⁸F]1, and that quantitative metrics of regional cardiac sympathetic nerve density can be obtained from tracer kinetic analyses of its myocardial kinetics.

Due to the different metabolic pathways of [¹⁸F]1 and [¹⁸F]2, both agents are currently being evaluated in first-in-human studies under an exploratory IND clearance from the FDA ([ClinicalTrials.gov](https://clinicaltrials.gov/ct2/show/study/NCT02385877), NCT02385877). The results of these studies will be used to select a lead radiotracer for further clinical development. If PET studies with one of these radiotracers can provide accurate and sensitive regional measures of cardiac sympathetic nerve density in human hearts, it could be used to investigate the contribution of cardiac sympathetic denervation to mechanisms that lead to sudden cardiac death from heart diseases. Based on previous clinical studies with [¹²³I]MIBG and [¹¹C]HED, a potential clinical role for [¹⁸F]1 or [¹⁸F]2 would be in improved risk stratification of heart failure patients being staged for implantable cardioverter defibrillator (ICD) therapy.

METHODS

Chemicals and General Instrumentation. NMR spectra were obtained on a Varian Inova 500 (499.90 MHz for ¹H; 125.70 MHz for ¹³C) spectrometer. ¹H and ¹³C NMR chemical shifts (δ) are reported in parts per million (ppm) relative to internal standard TMS and coupling constants (*J*) are in Hz. High-resolution mass spectra were obtained on a VG (Micromass) 70-250S spectrometer using electrospray ionization (ESI) in positive ion mode, direct chemical ionization (DCI) or electron impact (EI) at 70 eV. Melting points were determined on a Mel-Temp capillary melting point apparatus in open capillary tubes. Flash column chromatography was performed with E. Merck 230–400 mesh silica gel. Analytical TLC was performed with Analtech 0.25 mm glass-backed plates with fluorescent background. Visualization of TLC plates was achieved by UV illumination or treatment with phosphomolybdic acid (PMA). High pressure liquid chromatography (HPLC) was performed on a Hitachi pump L-7100 instrument equipped with Hitachi D-7500 integrator and Hitachi L-4000 UV detector. Radioactivity detection was done with Bioscan coincidence (model B-FC-4000) detector. Reverse-phase HPLC analysis of the formation of radiometabolites in plasma samples was performed on a PerkinElmer Series 410 LC instrument equipped with an Ortec model 905-4 NaI(Tl) radiodetector (Oak Ridge, TN).

Reagents and solvents were purchased from commercial sources and used without further purification unless otherwise noted. [¹⁹F]4F-MHPG and [¹⁹F]3F-PHPG (standards for HPLC analysis) and *N,N'*-bis(*tert*-butoxycarbonyl)-*N*-3-benzyloxy-4-iodophenethylguanidine (7) were prepared in our laboratory using previously reported methods.^{18,39}

N,N',N'',N'''-Tetrakis(*tert*-butoxycarbonyl)-*N*-3-benzyloxy-4-iodophenethylguanidine (8). A solution of di-*tert*-butyl dicarbonate (6.1 mmol, 6.1 mL of 1.0 M solution in THF) was added to a solution of *N,N'*-bis(*tert*-butoxycarbonyl)-*N*-3-benzyloxy-4-iodophenethylguanidine 7 (600 mg, 1.0 mmol), dimethylaminopyridine (74 mg, 0.61 mmol) and triethylamine (0.85 mL, 6.1 mmol) in anhydrous THF (12 mL) at room temperature. The mixture was stirred for 48 h and then poured over water (50 mL). The mixture was diluted with ethyl acetate (50 mL) and extracted with ethyl acetate (2 × 50 mL). The combined extracts were washed with brine, dried over Na₂SO₄ and concentrated under reduced pressure. The residue was purified by flash column chromatography (silica gel, 15% ethyl acetate in hexane) to afford the product 8 (730 mg, 92%) as a white oil; ¹H NMR (500 MHz, CDCl₃) δ 7.69 (d, *J* = 7.9 Hz, 1H), 7.53 (d, *J* = 7.4 Hz, 2H), 7.40 (t, *J* = 7.4 Hz, 2H), 7.32 (t, *J* = 7.4 Hz, 1H), 6.83 (d, *J* = 1.7 Hz, 1H), 6.66 (dd, *J* = 7.9, 1.7 Hz, 1H), 5.15 (s, 2H), 3.94 (td, *J* = 8.0, 4.9 Hz, 2H), 2.90 (td, *J* = 8.0, 4.9 Hz, 2H), 1.52–1.46 (m, 36H); ¹³C NMR (125 MHz, CDCl₃) δ 157.95, 157.48, 151.39, 147.63, 143.88, 141.05, 139.51, 136.74, 131.09, 128.72, 128.05, 127.40, 123.71, 113.89, 84.30, 83.92, 83.90, 82.29, 71.05, 48.78, 33.36, 28.25, 28.17, 28.13; MS (ESI) *m/z* 796 (M+H)⁺, HRMS (ESI) calcd for C₃₆H₅₀IN₃O₉ 818.2484 (M + Na)⁺, found 818.2491; Anal. Calcd For C₃₆H₅₀IN₃O₉: C, 54.34; H, 6.34; N, 5.28. Found: C, 54.54; H, 6.41; N, 5.14.

N,N',N'',N'''-Tetrakis(*tert*-butoxycarbonyl)-*N*-3-benzyloxy-4-trimethylstannylphenethyl Guanidine (9). Hexamethylditin (0.36 mL, 1.73 mmol) was added to a solution of compound 8 (688 mg, 0.86 mmol) and tetrakis(triphenylphosphine)palladium (50 mg, 0.04 mmol) in anhydrous toluene (8.0 mL) at room temperature under nitrogen atmosphere. The resulting mixture was heated to 130 °C for 30 min, cooled down to room temperature and filtered through a Celite pad. Celite pad was washed with ethyl acetate and the solvent was removed under reduced pressure. The residue was purified by flash column chromatography (silica gel, 100% hexane to 10% ethyl acetate in hexane) to afford the product 9 (621 mg, 86%) as a yellow oil; ¹H NMR (500 MHz, CDCl₃) δ 7.40–7.34 (m, 4H), 7.31–7.29 (m, 2H), 6.88 (d, *J* = 7.2 Hz, 1H), 6.82 (s, 1H), 5.02 (s, 2H), 3.96 (t, *J* = 8.1 Hz, 2H), 2.92 (t, *J* = 8.1 Hz, 2H), 1.53–1.31 (m, 36H), 0.17 (s, 9H); ¹³C NMR (126 MHz, CDCl₃) δ 158.0, 157.5, 151.4, 147.6, 143.9, 141.1, 139.5, 136.7, 128.7, 128.5, 127.4, 123.7, 113.9, 84.3, 83.9, 83.9, 82.3, 71.1, 48.8, 33.4, 28.3, 28.2, 28.1, 0.2; MS (ESI) *m/z* 834 (M + H)⁺, HRMS (ESI) calcd for C₃₉H₅₉N₃O₉Sn 856.3166 (M + Na)⁺, found 856.3183. Anal. Calcd For C₃₉H₅₉N₃O₉Sn: C, 56.26; H, 7.14; N, 5.05. Found: C, 56.00; H, 7.14; N, 4.88.

2-Benzyloxy-4-(2'-(*N,N',N'',N'''*-tetrakis(*tert*-butoxycarbonyl)-guanidinyloxy)ethyl)phenyl (2-thienyl)iodonium Tosylate (10). A solution of 2-(diacetoxy)iodothiophene (92 mg, 0.278 mmol) in CH₂Cl₂ (1.0 mL) was added to a solution of *p*-toluenesulfonic acid hydrate (53 mg, 0.278 mmol) in MeCN (1.0 mL) at room temperature under nitrogen atmosphere. The white precipitate was immediately generated, and the mixture was stirred for 1 h. A solution of compound 9 (232 mg, 0.278 mmol) in CH₂Cl₂ (1.0 mL) and MeCN (1.0 mL) was added slowly to the reaction mixture. After the white precipitate had disappeared, the mixture was stirred at room temperature for 20 h under nitrogen atmosphere. The solvent was removed under reduced pressure and the residue was purified by flash column chromatography (silica gel, 100% CH₂Cl₂ to 20:1 = CH₂Cl₂/MeOH) to afford the tosylate salt 10 (255 mg, 87%) as a yellow solid. mp 79–84 °C; ¹H NMR (500 MHz, DMSO-*d*₆) δ 8.26 (d, *J* = 8.1 Hz, 1H), 7.89 (dd, *J* = 5.3, 1.3 Hz, 1H), 7.76 (dd, *J* = 3.8, 1.3 Hz, 1H), 7.52–7.37 (m, 7H), 7.24 (d, *J* = 1.6 Hz, 1H), 7.11–7.08 (m, 3H), 6.95 (dd, *J* = 8.2, 1.6 Hz, 1H), 5.34 (s, 2H), 3.91 (t, *J* = 7.4 Hz, 2H), 2.91 (t, *J* = 7.4 Hz, 2H), 2.28 (s, 3H), 1.43–1.39 (m, 27H), 1.29 (s, 9H); ¹³C NMR (126 MHz, DMSO-*d*₆) δ 157.05, 155.10, 150.54, 146.676,

146.23, 145.82, 143.64, 139.44, 137.51, 136.87, 136.33, 135.67, 129.23, 128.63, 128.40, 128.01, 127.96, 127.28, 125.48, 123.77, 114.20, 108.08, 101.56, 83.43, 83.21, 81.51, 70.90, 48.86, 47.40, 46.17, 40.01, 32.64, 27.49, 27.41, 27.19, 20.77; HRMS (EI) calcd for $C_{40}H_{53}IN_3O_9S$ 878.2542 ($M - OTs$)⁺, found 878.2546.

2-Benzoyloxy-4-{2'-(*N,N,N',N'*-tetrakis(*tert*-butoxycarbonyl)-guanidiny)ethyl}phenyl (2-thienyl)iodonium Bromide (11). A solution of KBr (98 mg, 0.82 mmol) in H_2O (1.0 mL) was added to a solution of compound **10** (200 mg, 0.19 mmol) in MeCN (1.0 mL) at 60 °C for 5 min. The reaction mixture was stirred at room temperature for 1 h. The precipitate was washed with ice H_2O (10 mL), filtered, washed further with hexane several times, and dried in vacuo to afford the bromide salt **11** (156 mg, 86%) as a light yellow solid. mp 116–119 °C; 1H NMR (500 MHz, $DMSO-d_6$) δ 8.25 (d, J = 8.1 Hz, 1H), 7.86 (d, J = 5.3 Hz, 1H), 7.73 (d, J = 3.7 Hz, 1H), 7.52–7.38 (m, 5H), 7.22 (s, 1H), 7.08 (dd, J = 5.3, 3.7 Hz, 1H), 6.94 (d, J = 8.1 Hz, 1H), 5.33 (s, 2H), 3.91 (t, J = 7.4 Hz, 2H), 2.90 (t, J = 7.4 Hz, 2H), 1.43–1.39 (m, 27H), 1.30 (s, 9H); ^{13}C NMR (126 MHz, $DMSO-d_6$) δ 157.05, 155.06, 150.53, 146.73, 146.00, 143.63, 139.03, 136.90, 135.96, 135.70, 129.10, 128.61, 128.35, 127.92, 123.72, 114.17, 109.53, 108.87, 102.82, 83.43, 83.19, 81.49, 70.87, 47.38, 32.64, 27.48, 27.40, 27.20; HRMS (ESI) calcd for $C_{40}H_{53}IN_3O_9S$ 878.2542 ($M - Br$)⁺, found 878.2555. Anal. Calcd For $C_{40}H_{53}BrIN_3O_9S$: C, 50.11; H, 5.57; N, 4.38. Found: C, 50.04; H, 5.69; N, 4.37.

2-(4-Hydroxyphenyl)ethylamine *tert*-Butylcarbamate (13). To a solution of 2-(4-hydroxy phenyl)ethylamine **12** (4.00 g, 29.16 mmol) in THF (48 mL) was added triethylamine (4.3 mL, 30.82 mmol). Di-*tert*-butyl-dicarbonate (6.70 g, 30.70 mmol) was added to the resulting solution and the reaction mixture was stirred at room temperature overnight. The solvent was evaporated under reduced pressure and the residue was purified by flash column chromatography (silica gel, 20% ethyl acetate in hexane) to afford the desired compound **13** (6.78 g, 98%) as a colorless oil; 1H NMR (500 MHz, $CDCl_3$) δ 7.03 (d, J = 8.1 Hz, 2H), 6.77 (d, J = 8.1 Hz, 2H), 4.57 (br. s, NH), 3.33 (t, J = 6.5 Hz, 2H), 2.71 (t, J = 6.5 Hz, 2H), 1.47 (s, 9H); ^{13}C NMR (126 MHz, $CDCl_3$) δ 154.43, 129.88, 115.43, 98.46, 67.47, 42.01, 33.25, 28.46. CAS Registry Number: 64318-28-1.

2-(3-Iodo-4-hydroxyphenyl)ethylamine *tert*-Butylcarbamate (14). Sodium iodide (7.41 g, 49.45 mmol) and NaOH (1.54 g, 38.50 mmol) were added to a solution of compound **13** (7.82 g, 32.98 mmol) in MeOH (60 mL). The resulting solution was cooled to 0 °C. Sodium hypochlorite (4.0–4.9% in water, 81.8 mL, 49.45 mmol) was added slowly to the solution by dropping funnel. The reaction temperature was kept at 0–3 °C. After adding NaOCl, the reaction mixture was stirred for one more hour at 0–5 °C. A solution of sodium thiosulfate (10% in H_2O , 70 mL) was added, and the pH was adjusted to 6.5 by addition of HCl (2.0 N solution). The product was extracted by ethyl acetate (3 \times 100 mL), and the combined extracts were washed with brine, dried over Na_2SO_4 , and concentrated under reduced pressure. The residue was purified by flash column chromatography (silica gel, 20% ethyl acetate in hexane) to afford the compound **14** (5.15 g, 43%) as a white powder; mp 112–115 °C; 1H NMR (500 MHz, $CDCl_3$) δ 7.49 (s, 1H), 7.06 (d, J = 8.0 Hz, 1H), 6.92 (d, J = 8.0 Hz, 1H), 4.53 (br. s, NH), 3.31 (t, J = 6.5 Hz, 2H), 2.70 (t, J = 6.5 Hz, 2H), 1.47 (s, 9H); ^{13}C NMR (126 MHz, $CDCl_3$) δ 155.86, 153.51, 138.23, 133.11, 130.64, 115.02, 85.67, 79.40, 44.56, 34.78, 28.54. CAS Registry Number: 788824-50-0.

2-(4-Benzoyloxy-3-iodophenyl)ethylamine *tert*-Butylcarbamate (15). Benzyl bromide (0.52 g, 3.03 mmol) and K_2CO_3 (0.63 g, 4.55 mmol) were added to a solution of compound **14** (1.10 g, 3.03 mmol) in acetone (17 mL). The resulting solution was stirred at 70 °C for 4 h. The reaction mixture was filtered and the solvent was evaporated under reduced pressure. Water was added to the residue, the product was extracted by ethyl acetate (3 \times 100 mL), and the combined extracts were washed with brine, dried over Na_2SO_4 , and concentrated under reduced pressure. The residue was purified by flash column chromatography (silica gel, 10% ethyl acetate in hexane) to afford the compound **15** (1.07 g, 78%) as a white powder; mp 70–72 °C; 1H NMR (500 MHz, $CDCl_3$) δ 7.63 (s, 1H), 7.49 (d, J = 7.4 Hz, 2H), 7.39 (t, J = 7.4 Hz, 2H), 7.32 (t, J = 7.4 Hz, 1H), 7.09 (d, J = 8.3 Hz,

1H), 6.79 (d, J = 8.3 Hz, 1H), 5.13 (s, 2H), 4.52 (br. s, NH), 3.32 (t, J = 6.5 Hz, 2H), 2.70 (t, J = 6.5 Hz, 2H), 1.44 (s, 9H); ^{13}C NMR (126 MHz, $CDCl_3$) δ 155.90, 155.80, 139.67, 136.56, 133.56, 130.87, 128.79, 128.54, 127.86, 126.98, 112.72, 86.92, 79.33, 70.97, 41.78, 34.80, 28.45, 28.41. CAS Registry Number: 788824-73-7.

2-(4-Benzoyloxy-3-iodophenyl)ethylamine Hydrochloride (16). Hydrochloric acid (45 mL of 4.0 M solution in 1,4-dioxane, 180 mmol) was added to a solution of compound **15** (0.80 g, 17.6 mmol) in ethyl acetate (5 mL). The resulting solution was stirred at 65 °C for 1 h. The solvent was evaporated under reduced pressure. The crude product was dissolved again in ethyl acetate and concentrated under reduced pressure. The residue was purified by flash column chromatography (silica gel, 5% methanol, and 0.3% NH_4OH in methylene chloride) to afford the compound **16** (0.61 g, 97%) as a yellow powder; mp 162–167 °C; 1H NMR (500 MHz, $CDCl_3$) δ 7.70 (s, 1H), 7.46 (d, J = 7.4 Hz, 2H), 7.37 (t, J = 7.4 Hz, 2H), 7.30 (t, J = 7.4 Hz, 1H), 7.15 (d, J = 8.4 Hz, 1H), 6.76 (d, J = 8.4 Hz, 1H), 5.07 (s, 2H), 3.20 (t, J = 7.8 Hz, 2H), 3.00 (t, J = 7.8 Hz, 2H); ^{13}C NMR (126 MHz, $CDCl_3$) δ 156.50, 139.75, 136.35, 130.52, 129.83, 128.55, 127.89, 126.97, 112.91, 110.01, 87.48, 87.22, 70.92, 45.82, 41.12. CAS Registry Number: 794507-50-9.

***N,N'*-Bis(*tert*-butoxycarbonyl)-*N*-4-benzoyloxy-3-iodophenethylguanidine (17).** To a cooled (0 °C) solution of compound **16** (0.37 g, 1.06 mmol) and triethylamine (0.75 mL, 5.38 mmol) in anhydrous DMF (3.5 mL) was added in portion 1,3-bis(*tert*-butoxycarbonyl)-2-methyl-2-thiopseudourea (0.34 g, 1.16 mmol). The resulting mixture was stirred at 0 °C for 1 h, warmed to room temperature and stirred overnight. The mixture was diluted with ethyl acetate (50 mL), washed with saturated NH_4Cl solution (200 mL), and extracted with ethyl acetate (2 \times 150 mL). The combined extracts were washed with brine, dried over Na_2SO_4 , and concentrated under reduced pressure. The residue was purified by flash column chromatography (silica gel, 10% ethyl acetate in hexane) to afford the product **17** (0.37 g, 58%) as a white solid; mp 115–117 °C; 1H NMR (500 MHz, $CDCl_3$) δ 11.46 (br. s, 1NH), 8.38 (br. s, 1NH), 7.67 (s, 1H), 7.49 (d, J = 7.6 Hz, 2H), 7.39 (t, J = 7.6 Hz, 2H), 7.32 (t, J = 7.6 Hz, 1H), 7.11 (d, J = 9.0 Hz, 1H), 6.78 (d, J = 9.0 Hz, 1H), 5.13 (s, 2H), 3.62 (q, J = 6.7 Hz, 2H), 2.77 (t, J = 6.7 Hz, 2H), 1.50 (s, 18H); ^{13}C NMR (126 MHz, $CDCl_3$) δ 156.11, 155.99, 139.76, 136.57, 133.15, 129.69, 128.53, 127.84, 126.98, 112.74, 86.91, 83.12, 79.26, 70.96, 42.15, 33.93, 28.31, 28.09; HRMS calcd for $C_{26}H_{34}IN_3O_5$ 596.1616, found 596.1615.

***N,N',N'',N''*-Tetrakis(*tert*-butoxycarbonyl)-*N*-4-benzoyloxy-3-iodophenethylguanidine (18).** A solution of di-*tert*-butyl dicarbonate (40.7 mmol, 40.7 mL of 1.0 M solution in THF) was added to a solution of compound **17** (4.04 g, 6.78 mmol), *N,N*-dimethylaminopyridine (497 mg, 4.07 mmol), and triethylamine (5.67 mL, 40.1 mmol) in anhydrous THF (82 mL) at room temperature. The mixture was stirred for 48 h and then poured over water (200 mL). The mixture was diluted with ethyl acetate (200 mL). After decantation, the aqueous layer was extracted with ethyl acetate (2 \times 200 mL). The combined extracts were washed with brine, dried over Na_2SO_4 , and concentrated under reduced pressure. The residue was purified by flash column chromatography (silica gel, 10% ethyl acetate in hexane) to afford the product **18** (3.41 g, 63%) as a white oil; 1H NMR (500 MHz, $CDCl_3$) δ 7.71 (s, 1H), 7.49 (d, J = 7.6 Hz, 2H), 7.39 (t, J = 7.6 Hz, 2H), 7.32 (t, J = 7.6 Hz, 1H), 7.17 (d, J = 8.4 Hz, 1H), 6.78 (d, J = 8.4 Hz, 1H), 5.13 (s, 2H), 3.93 (t, J = 8.0 Hz, 2H), 2.85 (t, J = 8.0 Hz, 2H), 1.50 (s, 36H); ^{13}C NMR (126 MHz, $CDCl_3$) δ 157.68, 155.85, 147.34, 139.77, 136.58, 133.51, 129.92, 128.54, 127.85, 126.98, 112.71, 86.84, 83.66, 82.03, 70.96, 48.73, 31.87, 28.04, 27.98, 27.91; HRMS calcd for $C_{36}H_{50}IN_3O_9$ 818.2484, found 818.2479.

***N,N',N'',N''*-Tetrakis(*tert*-butoxycarbonyl)-*N*-4-benzoyloxy-3-trimethylstannylphenethylguanidine (19).** Hexamethylditin (2.0 mL, 9.60 mmol) was added to a solution of compound **18** (2.79 g, 3.50 mmol) and tetrakis(triphenylphosphine)palladium (200 mg, 0.16 mmol) in anhydrous toluene (30 mL) at room temperature under nitrogen atmosphere. The resulting mixture was heated to 130 °C for 30 min, cooled down to room temperature, and filtered through a Celite pad. Celite pad was washed with ethyl acetate and the solvent was removed under reduced pressure. The residue was purified by flash column

chromatography (silica gel, 100% hexane to 10% ethyl acetate in hexane) to afford the product **19** (2.87, 98%) as a yellow oil; ^1H NMR (500 MHz, CDCl_3) δ 7.42–7.37 (m, 4H), 7.32 (t, J = 6.5 Hz, 2H), 6.91 (d, J = 7.1 Hz, 1H), 6.84 (s, 1H), 5.04 (s, 2H), 3.98 (t, J = 8.1 Hz, 2H), 2.94 (t, J = 8.1 Hz, 2H), 1.51–1.49 (m, 36H), 0.19 (s, 9H); ^{13}C NMR (126 MHz, CDCl_3) δ 163.2, 157.8, 151.2, 147.4, 143.6, 141.2, 137.1, 136.5, 128.4, 128.1, 127.8, 127.7, 121.8, 110.9, 83.6, 83.4, 82.0, 70.0, 48.9, 33.6, 28.1, 28.0, 27.9, 14.1; HRMS (ESI) calcd for $\text{C}_{39}\text{H}_{59}\text{N}_3\text{O}_9\text{Sn}$ 856.3166 ($\text{M}+\text{Na}$) $^+$, found 856.3172. Anal. Calcd For $\text{C}_{39}\text{H}_{59}\text{N}_3\text{O}_9\text{Sn}$: C, 56.26; H, 7.14; N, 5.05. Found: C, 56.00; H, 7.23; N, 4.90.

2-Benzyloxy-5-[2'-(N,N',N'',N'' -tetrakis(*tert*-butoxycarbonyl)-guanidiny]ethyl]phenyl(2-thienyl)iodonium Tosylate (20**).** A solution of 2-(diacetoxyl)iodothiophene (209 mg, 0.637 mmol) in CH_2Cl_2 (5.0 mL) was added to a solution of *p*-toluenesulfonic acid hydrate (121 mg, 0.637 mmol) in MeCN (5.0 mL) at room temperature under nitrogen atmosphere. The white precipitate was immediately generated and the mixture was stirred for 1 h. A solution of compound **19** (530 mg, 0.637 mmol) in CH_2Cl_2 (3.0 mL) and MeCN (3.0 mL) was added slowly to the reaction mixture. After the white precipitate disappeared, the mixture was stirred at room temperature for 20 h under nitrogen atmosphere. The solvent was removed under reduced pressure, and the residue was purified by flash column chromatography (silica gel, 100% CH_2Cl_2 to 20:1 = CH_2Cl_2 /MeOH) to afford the tosylate salt **20** (482 mg, 86%) as a yellow solid; mp 140–141 $^\circ\text{C}$; ^1H NMR (500 MHz, $\text{DMSO}-d_6$) δ 8.21 (s, 1H), 7.90 (t, J = 5.3 Hz, 1H), 7.77 (t, J = 5.3 Hz, 1H), 7.49–7.37 (m, 7H), 7.32 (d, J = 8.5 Hz, 2H), 7.12–7.08 (m, 3H), 5.33 (s, 2H), 3.88 (t, J = 7.8 Hz, 2H), 2.85 (t, J = 7.8 Hz, 2H), 2.28 (s, 3H), 1.43–1.36 (m, 36H); ^{13}C NMR (126 MHz, $\text{DMSO}-d_6$) δ 157.1, 153.7, 150.6, 146.7, 145.8, 143.6, 139.5, 137.5, 136.5, 136.3, 135.8, 134.7, 133.7, 129.2, 128.6, 128.3, 128.0, 127.7, 125.5, 113.9, 110.3, 101.3, 83.6, 83.2, 81.6, 70.9, 47.5, 31.1, 27.9, 27.52, 27.4, 27.3, 27.2, 20.9.

2-Benzyloxy-5-[2'-(N,N',N'',N'' -tetrakis(*tert*-butoxycarbonyl)-guanidiny]ethyl]phenyl(2-thienyl)iodonium Bromide (21**).** A solution of KBr (583 mg, 4.90 mmol) in H_2O (5.0 mL) was added to a solution of compound **20** (430 mg, 0.49 mmol) in MeCN (7.0 mL) at 60 $^\circ\text{C}$ for 5 min. The reaction mixture was stirred at room temperature for 1 h. The precipitate was washed with ice H_2O (10 mL), filtered, washed further with hexane several times, and dried in vacuo to afford the bromide salt **21** (411 mg, 96%) as a light yellow solid; mp 140–141 $^\circ\text{C}$; ^1H NMR (500 MHz, CDCl_3) δ 7.97 (s, 1H), 7.53 (d, J = 5.2 Hz, 1H), 7.46 (d, J = 5.2 Hz, 1H), 7.41–7.35 (m, 6H), 6.96–6.91 (m, 2H), 5.21 (s, 2H), 3.92 (t, J = 8.1 Hz, 2H), 2.90 (t, J = 8.1 Hz, 2H), 1.52–1.48 (m, 36H); ^{13}C NMR (126 MHz, CDCl_3) δ 157.6, 153.6, 151.1, 147.3, 143.5, 137.9, 136.5, 135.2, 134.7, 134.6, 133.8, 128.8, 128.7, 128.5, 127.5, 114.4, 113.8, 83.89, 83.8, 82.2, 71.9, 48.4, 33.8, 32.0, 29.7, 28.1, 28.0, 27.9; HRMS (ESI) calcd for $\text{C}_{40}\text{H}_{53}\text{BrN}_3\text{O}_9\text{S}$ 878.2542 ($\text{M}-\text{Br}$) $^+$, found 878.2540. Anal. Calcd For $\text{C}_{40}\text{H}_{53}\text{BrN}_3\text{O}_9\text{S}$: C, 50.11; H, 5.57; N, 4.38. Found: C, 51.86; H, 5.95; N, 4.24.

Radiosynthesis of [^{18}F]1**.** A TRACERlab FX_{FN} computer-controlled radiosynthesis module (GE Healthcare) was used to achieve fully automated radiosyntheses of [^{18}F]**1** and [^{18}F]**2**. [^{18}F] F^- was prepared by the $^{18}\text{O}(p,n)^{18}\text{F}$ reaction using H_2^{18}O as the target material in a GE PETrace cyclotron. [^{18}F] F^- was isolated from the enriched water by trapping on a Waters Sep-Pak Light QMA cartridge (preactivated with 10 mL of ethanol and 10 mL of H_2O) and eluted from the cartridge into the glassy-carbon reactor vial of the TRACERlab FX_{FN} system with a solution of 0.5 mL Cs_2CO_3 (0.05 M in H_2O). MeCN (1.0 mL) was added to the reactor vessel and then water/acetonitrile was evaporated at 80 $^\circ\text{C}$ under vacuum with a nitrogen stream to yield dried Cs^{18}F . After cooling to 60 $^\circ\text{C}$, a mixed solution of 0.5 mL of DMF and 20 μL of Milli-Q H_2O , containing 5.5–6.0 mg of the diaryliodonium salt precursor **11** and 1.0 mg of TEMPO (2,2,6,6-tetramethylpiperidine-*N*-oxyl) were added to the reactor vessel containing Cs^{18}F . The sealed reaction mixture was heated at 150 $^\circ\text{C}$ for 5 min to produce 3-benzyloxy-4-[^{18}F]fluorophenethyl- N,N',N'',N'' -tetrakis-BOC-guanidine [^{18}F]**22** as intermediate. After cooling to 70 $^\circ\text{C}$, a solution of 48% HBr (0.5 mL) and MeCN (0.5 mL) was added to the reaction mixture. The reaction

solution was heated at 120 $^\circ\text{C}$ for 15 min and then cooled to 50 $^\circ\text{C}$. Next, a mixture solution of NaOH solution (1.0 mL, 4.0 M in H_2O) and buffer solution (1.8 mL, 5% EtOH in 40 mM NH_4OAc) was added into the reactor vessel. This mixture was injected onto a reverse-phase HPLC column (Phenomenex Synergi 10 μ Hydro-RP 80A, 250 \times 10 mm, 5% EtOH in 40 mM NH_4OAc buffer, flow rate 4.0 mL/min, λ = 254 nm) and [^{18}F]**1** was collected at R_t = 30–32 min. The collected [^{18}F]**1** fraction was passed through a 0.22 μm sterilizing filter directly into a 10 mL septum-sealed sterile pyrogen-free glass vial.

Specific activity (SA) was determined by injecting a sample of [^{18}F]**1** with known activity (kBq) onto an HPLC system used for quality control. The area under the UV absorbance peak associated with the [^{18}F]**1** radioactivity peak was compared against a predetermined standard curve to estimate the total mass ([^{18}F]**4F-MHPG** + [^{19}F]**4F-MHPG**) in micrograms. The ratio of ^{18}F -activity to total mass (converted from μg to μmol using the molecular weight of [^{19}F]**4F-MHPG**) gave the specific activity.

Radiosynthesis of [^{18}F]2**.** The same methods described for the synthesis of [^{18}F]**1** were used to prepare [^{18}F]**2**, except that the appropriate precursor **21** was used instead of precursor **11**. HPLC purification conditions were slightly different: Phenomenex Synergi 10 μ Hydro-RP 80A, 250 \times 10 mm, 3.5% EtOH in 40 mM NH_4OAc buffer, flow rate 4.0 mL/min, λ = 254 nm. In this system, [^{18}F]**2** was collected at R_t = 31–33 min.

Isolated Rat Heart Studies. Hearts from male Sprague–Dawley rats (225–500 g) were perfused under moderate workload conditions (7.3 mmHg preload, 73 mmHg afterload) using a working heart preparation.⁴⁰ Two parallel perfusion circuits were connected to the left atrial cannula with a three-way connector to allow for rapid switching from one circuit to the other. The heart perfusate was Krebs–Henseleit (KH) bicarbonate buffer (118 mM NaCl, 4.7 mM KCl, 2.55 mM CaCl_2 , 1.2 mM MgSO_4 , 1.2 mM KH_2PO_4 , and 25 mM NaHCO_3) containing 5 mM glucose, oxygenated with a 95% O_2 /5% CO_2 gas mixture and held at 37 $^\circ\text{C}$. Corticosterone (54 μM) was added to the perfusate to block extraneuronal uptake (uptake-2) of the radiotracer into the rat myocardium.²³

Fluorine-18 activity in the heart was measured externally using a pair of cesium fluoride (CsF) scintillation detectors with crystal size 51 cm diameter and 51 cm thick (Crismatec 51Y51; Saint-Gobain, Nemours, France). The front faces of the two CsF detectors were positioned directly opposite each other, \sim 4 cm apart, with the heart centered between them. Each detector was enclosed in a large cylindrical lead collimator (2 cm wall thickness, 25 cm long) to shield against background counts from radioactive sources outside the heart. Two coincidence detection circuits were established between the detectors using standard Nuclear Instrumentation Module (NIM) electronic modules. One circuit measured total coincident events between the two detectors (true + random coincident events), and the second measured only random coincident events. A computerized data acquisition system interfaced to the NIM-module coincidence circuits was used to acquire and record the whole-heart radioactivity data throughout the study.⁴¹

Hearts were initially perfused for a 30 min stabilization period using KH buffer in the first perfusion circuit. During this time, [^{18}F]**2** was added to 1.0 L of KH buffer circulating in the second perfusion circuit and allowed to equilibrate over several minutes. Three 1.0 mL aliquots were drawn from the second perfusion circuit for counting in a gamma counter (Cobra II Auto-Gamma, PerkinElmer, Waltham, MA) to determine the radioactivity concentration in the perfusate (C_p), which was \sim 74 kBq/mL perfusate. After initiating data acquisition from the CsF detectors, the heart was rapidly switched to the second perfusion circuit to begin a constant infusion of [^{18}F]**2** for 10 min. Then the heart was switched back to the first perfusion circuit for 120 min to measure clearance rates of the tracer from the heart.

The acquired whole-heart radioactivity data (counts per second; cps) at each time point were converted to an “apparent distribution volume” (ADV; mL perfusate/g wet), by dividing by the perfusate radioactivity concentration C_p (kBq/mL perfusate), the detector system calibration factor Z_{calib} (cps/kBq), and the measured wet mass of the heart M_w (g wet). Neuronal uptake rates of the radiotracers

(K_{up} ; mL perfusate/min/g wet) were calculated as the slope of a linear regression of the ADV data between $t = 1$ min and $t = 4$ min of the 10 min infusion study. Clearance rates were estimated by fitting the ADV data during the clearance phase of the study to multiple exponential decay processes. The exponential clearance rate constants (λ_i) were used to calculate corresponding clearance half-times: $T_{1/2} = \ln(2)/\lambda_i$. The slowest rate, associated with clearance from sympathetic neurons, is reported for each compound.

PET Imaging Studies with [^{18}F]2. Cardiac PET studies ($n = 4$) were performed in rhesus macaque monkeys using a microPET P4 primate scanner (Siemens/CTI Concorde Microsystems, Knoxville, TN). After anesthetizing the animal, a percutaneous angiocatheter was placed in the saphenous vein of each leg, one for tracer injection, the other for blood sampling. Vital signs, including heart rate (bpm), blood oxygen saturation levels (SpO_2) and body temperature were monitored continuously (model V3404P, SurgiVet, Norwell, MA). Dynamic PET data were acquired in list-mode for 90 min after intravenous injection of 155–230 MBq of [^{18}F]2. List-mode emission data were rebinned into a 27-frame dynamic sequence (12×10 s, 2×30 s, 2×60 s, 2×150 s, 2×300 s, 7×600 s). Rebinning emission data were corrected for attenuation and scatter, and transaxial images reconstructed using maximum a posteriori (MAP) reconstruction,⁴² an iterative method that accounts for the detector point spread function in the model of the system.

Blood Partitioning and Radiometabolite Analysis. Venous blood samples (1.5–2.0 mL) were centrifuged for 1 min at 12 000g to separate plasma and red blood cells. Plasma was deproteinized by adding perchloric acid (HClO_4 ; final concentration 0.4 N) and centrifuging for 5 min at 12 000g. The supernatant was neutralized with KOH (pH 7.0–7.5) and filtered twice (Millex GS 0.22 μm , Millipore, Billerica, MA). Aliquots (0.1 mL) of whole blood, plasma, and the final supernatant were counted in a gamma counter. Count data for plasma and whole blood aliquots were decay corrected and used to calculate the relative concentrations of [^{18}F]2 in plasma and whole blood (C_p/C_{wb}). The final supernatant was analyzed by HPLC (Synergi 10 μm Hydro-RP column, 4.6×250 mm, 60 mM sodium phosphate buffer, pH 5.4 with 8% ethanol, flow rate 1.0 mL/min) with an in-line radiation detector. Under the HPLC conditions used, [^{18}F]2 had a retention time $R_t = 12.7$ min, while the main polar radiometabolite formed had $R_t = 9.3$ min. Peak area analysis of the radiation detection curve was used to estimate the percentage intact parent tracer fraction (f_{intact}) for each plasma sample.

In Vitro Metabolism Tests. To test for sulfate conjugation of [^{18}F]2, a 20 μL aliquot of monkey liver cytosol (#452461, BD Biosciences, San Jose, CA) was added to a 10 μL aliquot of 10 mM sulfotransferase cofactor PAPS (adenosine-3'-phosphate-5'-phosphosulfate lithium salt hydrate; #A1651, Sigma-Aldrich, Milwaukee, WI) dissolved in 50 μL of 1.0 mM Tris-HCl buffer (pH 7.4) and 170 μL of ultrapure water (18 M Ω -cm Milli-Q, Millipore, Billerica, MA) and incubated at 37 $^\circ\text{C}$ for 5 min.⁴³ Next, 740 kBq of [^{18}F]2 in 250 μL of ultrapure water was added to the reaction mixture (final volume 500 μL) and incubated at 37 $^\circ\text{C}$ for 20 min. The reaction was terminated by centrifugation at 16 000g for 5 min at 4 $^\circ\text{C}$. The supernatant was filtered (Millex GS 0.22 μm , Millipore, Billerica, MA) and analyzed using HPLC with radiation detection as described above for the rhesus macaque plasma samples. To test for glucuronidation of [^{18}F]2, a 25 μL aliquot containing 0.5 mg of monkey liver microsomes (#452413, BD Biosciences, San Jose, CA) was added to a reaction mixture of 50 μL of 20 mM glucuronidation cofactor UDPGA (uridine 5'-diphosphoglucuronic acid; #U5625 Sigma-Aldrich, Milwaukee, WI) and 50 μL of 30 mM DTT (dithiothreitol, #D0632, Sigma-Aldrich, Milwaukee, WI) dissolved in 1.0 M glycine/NaOH buffer containing 50 mM MgCl_2 (pH 9.2). An additional 125 μL of the glycine/NaOH buffer was added and the mixture incubated at 37 $^\circ\text{C}$ for 5 min. Next, 740 kBq of [^{18}F]2 in 250 μL of ultrapure water was added to the reaction mixture (final volume 500 μL) and incubated at 37 $^\circ\text{C}$ for 20 min. Using the same procedures for the sulfate conjugation test, the reaction mixture was centrifuged and the supernatant filtered for analysis using radio-HPLC.

Plasma Time–Activity Curve. Region-of-interest analysis of the dynamic PET images was used to determine a time-activity curve of the activity concentration in whole blood, $C_{wb}(t)$. The whole blood time-activity curve $C_{wb}(t)$ was then multiplied by the measured ratio of activity in plasma over whole blood (C_p/C_{wb}) and by the percentage of intact parent tracer fraction in plasma data, $f_{\text{intact}}(t)$, to estimate the kinetics of the plasma concentration of intact tracer, $C_p(t)$. The estimated plasma curve $C_p(t)$ was used as the input function for tracer kinetic analyses.

Tracer Kinetic Analysis. For each PET study, the final four dynamic image frames were summed and used to draw a region-of-interest in the left ventricular wall, encompassing three to four transaxial slices, to extract a time-activity curve for myocardial tissue $C_t(t)$. For compartmental modeling analysis, $C_t(t)$ and the plasma kinetics $C_p(t)$ for [^{18}F]2 were analyzed using a two-tissue compartment model with irreversible trapping to estimate the rate constants K_1 (mL/min/g), k_2 (min^{-1}), k_3 (min^{-1}) and a blood volume fraction BV (dimensionless). The $C_t(t)$ and $C_p(t)$ data were also analyzed using Patlak analysis to estimate a Patlak slope, K_p (mL/min/g).

Animal Care. The care of all animals used in this study was done in accordance with the Animal Welfare Act and the National Institute of Health's Guide for the Care and use of Laboratory Animals.⁴⁴ Animal protocols were approved by the Institutional Animal Care and Use Committee (IACUC) at the University of Michigan.

AUTHOR INFORMATION

Corresponding Author

*Mailing address: Division of Nuclear Medicine, Department of Radiology, 2276 Medical Science I Bldg, SPC-5610, University of Michigan Medical School, Ann Arbor, MI 48109, USA. Telephone: 734-936-0725. Fax: 734-764-0288. E-mail: raffel@umich.edu.

ORCID

David M. Raffel: 0000-0002-7188-9463

Author Contributions

D.M.R. and Y.-W.J. designed the tracers; Y.-W.J., K.S.J., and D.M.R. developed the radiosynthetic approach; Y.-W.J. and K.S.J. prepared the radiosynthetic precursors and the non-radioactive standards for HPLC, and performed all radio-syntheses; D.M.R. performed the isolated rat heart studies; P.S.S., C.A.Q., G.G., Y.-W.J., and D.M.R. performed the PET imaging studies; D.M.R. performed the PET image analysis and kinetic data analysis with contributions from R.A.K.; G.G., D.M.R., and Y.-W.J. performed all metabolism studies.

Funding

We gratefully acknowledge the support of this work through PHS Grant R01-HL079540 from the National Heart Lung and Blood Institute, National Institutes of Health, Bethesda, MD.

Notes

The authors declare no competing financial interest.

ACKNOWLEDGMENTS

The authors thank the staff of the University of Michigan Cyclotron Facility for their many contributions to this study.

ABBREVIATIONS USED

DMI, desipramine; [^{11}C]HED, [^{11}C]-(-)-*m*-hydroxyephedrine; [^{11}C]GMO, *N*-[^{11}C]guanyl-(-)-*m*-octopamine; [^{123}I]MIBG, [^{123}I]-*m*-iodobenzylguanidine; NET, norepinephrine transporter; TEMPO, 2,2,6,6-tetramethylpiperidine-*N*-oxyl; VMAT2, vesicular monoamine transporter, isoform 2

■ REFERENCES

- (1) Fukuda, K., Kanazawa, H., Aizawa, Y., Ardell, J. L., and Shivkumar, K. (2015) Cardiac innervation and sudden cardiac death. *Circ. Res.* 116, 2005–2019.
- (2) Shen, M. J., and Zipes, D. P. (2014) Role of the autonomic nervous system in modulating cardiac arrhythmias. *Circ. Res.* 114, 1004–1021.
- (3) Kuehl, M., and Stevens, M. J. (2012) Cardiovascular autonomic neuropathies as complications of diabetes mellitus. *Nat. Rev. Endocrinol.* 8, 405–416.
- (4) Floras, J. S. (1993) Clinical aspects of sympathetic activation and parasympathetic withdrawal in heart failure. *J. Am. Coll. Cardiol.* 22 (4 Suppl. A), 72A–82A.
- (5) Baker, A. J. (2014) Adrenergic signaling in heart failure: a balance of toxic and protective effects. *Pflugers Arch.* 466, 1139–1150.
- (6) Gardner, R. T., Ripplinger, C. M., Myles, R. C., and Habecker, B. A. (2016) Molecular mechanisms of sympathetic remodeling and arrhythmias. *Circ.: Arrhythmia Electrophysiol.* 9, e001359.
- (7) Vaseghi, M., and Shivkumar, K. (2008) The role of the autonomic nervous system in sudden cardiac death. *Prog. Cardiovasc. Dis.* 50, 404–419.
- (8) Zipes, D. P., and Rubart, M. (2006) Neural modulation of cardiac arrhythmias and sudden cardiac death. *Heart Rhythm* 3, 108–113.
- (9) Henneman, M. M., Bengel, F. M., van der Wall, E. E., Knuuti, J., and Bax, J. J. (2008) Cardiac neuronal imaging: application in the evaluation of cardiac disease. *J. Nucl. Cardiol.* 15, 442–455.
- (10) Wollenweber, T., and Bengel, F. M. (2014) Molecular imaging to predict ventricular arrhythmia in heart failure. *J. Nucl. Cardiol.* 21, 1096–1109.
- (11) Wieland, D. M., Brown, L. E., Rogers, W. L., Worthington, K. C., Wu, J.-L., Clinthorne, N. H., Otto, C. A., Swanson, D. P., and Beierwaltes, W. H. (1981) Myocardial imaging with a radioiodinated norepinephrine storage analog. *J. Nucl. Med.* 22, 22–31.
- (12) Rosenspire, K. C., Haka, M. S., Van Dort, M. E., Jewett, D. M., Gildersleeve, D. L., Schwaiger, M., and Wieland, D. M. (1990) Synthesis and preliminary evaluation of carbon-11-meta-hydroxyephedrine: a false transmitter agent for heart neuronal imaging. *J. Nucl. Med.* 31, 1328–1334.
- (13) Jacobson, A. F., Senior, R., Cerqueira, M. D., Wong, N. D., Thomas, G. S., Lopez, V. A., Agostini, D., Weiland, F., Chandna, H., and Narula, J. (2010) Myocardial iodine-123 meta-iodobenzylguanidine imaging and cardiac events in heart failure: results of the prospective ADMIRE-HF (AdreView Myocardial Imaging for Risk Evaluation in Heart Failure) study. *J. Am. Coll. Cardiol.* 55, 2212–2221.
- (14) Fallavollita, J. A., Heavey, B. M., Luisi, A. J., Michalek, S. M., Baldwa, S., Mashtare, T. L., Hutson, A. D., DeKemp, R. A., Haka, M. S., Sajjad, M., Cimato, T. R., Curtis, A. B., Cain, M. E., and Canty, J. M. (2014) Regional myocardial sympathetic denervation predicts the risk of sudden cardiac arrest in ischemic cardiomyopathy. *J. Am. Coll. Cardiol.* 63, 141–149.
- (15) Deyell, M. W., Krahn, A. D., and Goldberger, J. J. (2015) Sudden cardiac death risk stratification. *Circ. Res.* 116, 1907–1918.
- (16) Raffel, D. M., Jung, Y. W., Gildersleeve, D. L., Sherman, P. S., Moskwa, J. J., Tluczek, L. J., and Chen, W. (2007) Radiolabeled phenethylguanidines: novel imaging agents for cardiac sympathetic neurons and adrenergic tumors. *J. Med. Chem.* 50, 2078–2088.
- (17) Raffel, D. M., Koeppe, R. A., Jung, Y. W., Gu, G., Jang, K. S., Sherman, P. S., and Quesada, C. A. (2013) Quantification of cardiac sympathetic nerve density of N - ^{11}C -guanyl-meta-octopamine and tracer kinetic analysis. *J. Nucl. Med.* 54, 1645–1652.
- (18) Jang, K. S., Jung, Y. W., Gu, G., Koeppe, R. A., Sherman, P. S., Quesada, C. A., and Raffel, D. M. (2013) 4- ^{18}F -fluoro- m -hydroxyphenethylguanidine: a radiopharmaceutical for quantifying regional cardiac sympathetic nerve density with positron emission tomography. *J. Med. Chem.* 56, 7312–7323.
- (19) Jang, K. S., Jung, Y. W., Song, H. C., and Raffel, D. M. (2015) Strategies for radiolabeling of 4- ^{18}F -fluoro- m -hydroxyphenethylguanidine ([^{18}F]4F-MHPG): a novel imaging agent for cardiac sympathetic innervation. *Mol. Imaging Biol.* 17 (Suppl 1), S997.
- (20) Kazmierczak, P., Skulski, L., and Kraszkiewicz, L. (2001) Synthesis of (diacetoxyiodo)arenes or iodylarenes from iodoarenes, with sodium periodate as the oxidant. *Molecules* 6, 881–891.
- (21) Chun, J.-H., and Pike, V. W. (2012) Regiospecific syntheses of functionalized diaryliodonium tosylates via [hydroxy(tosyloxy)iodo]-arenes generated in situ from (diacetoxyiodo)arenes. *J. Org. Chem.* 77, 1931–1938.
- (22) Ross, T. L., Ermert, J., Hocke, C., and Coenen, H. H. (2007) Nucleophilic ^{18}F -fluorination of heteroaromatic iodonium salts with no-carrier-added [^{18}F]fluoride. *J. Am. Chem. Soc.* 129, 8018–8025.
- (23) Salt, P. J. (1972) Inhibition of noradrenaline uptake₂ in the isolated rat heart by steroids, clonidine and methoxylated phenethylamines. *Eur. J. Pharmacol.* 20, 329–340.
- (24) Schäfer, M. K. H., Weihe, E., and Eiden, L. E. (2013) Localization and expression of VMAT2 across mammalian species: a translational guide for its visualization and targeting in health and disease. *Adv. Pharmacol.* 68, 319–334.
- (25) DeGrado, T. R., Hutchins, G. D., Toorongan, S. A., Wieland, D. M., and Schwaiger, M. (1993) Myocardial kinetics of carbon-11-meta-hydroxyephedrine: retention mechanisms and effects of norepinephrine. *J. Nucl. Med.* 34, 1287–1293.
- (26) Raffel, D. M., and Wieland, D. M. (2001) Assessment of cardiac sympathetic nerve integrity with positron emission tomography. *Nucl. Med. Biol.* 28, 541–559.
- (27) Raffel, D. M. (2012) Targeting norepinephrine transporters in cardiac sympathetic nerve terminals. In *Targeted Molecular Imaging* (Welch, M. J., and Eckelman, W. C., Eds.), pp 305–320, CRC Press, Boca Raton, FL.
- (28) Patlak, C. S., and Blasberg, R. G. (1985) Graphical evaluation of blood-to-brain transfer constants from multiple-time uptake data. Generalizations. *J. Cereb. Blood Flow Metab.* 5, 584–590.
- (29) Costa, E., Kuntzman, R., Gessa, G. L., and Brodie, B. B. (1962) Structural requirements for bretylium and guanethidine-like activity in a series of guanidine derivatives. *Life Sci.* 1, 75–80.
- (30) Fielden, R., and Green, A. L. (1965) The effects of some aralkylguanidines in mice. *Br. J. Pharmacol. Chemother.* 24, 408–417.
- (31) Green, A. L., Fielden, R., Bartlett, D. C., Cozens, M. J., Eden, R. J., and Hills, D. W. (1967) New norepinephrine-depleting agents. β -hydroxyphenethylguanidine and related compounds. *J. Med. Chem.* 10, 1006–1008.
- (32) Maxwell, R. A., and Wastila, W. B. (1977) Adrenergic Neuron Blocking Drugs. In *Antihypertensive Agents. Handbook of Pharmacology XXXIX* (Gross, F., Ed.), pp 161–211, Springer-Verlag, New York.
- (33) Raffel, D. M. (2015) Preclinical evaluations of cardiac sympathetic innervation radiotracers. In *Autonomic Innervation of the Heart: Role of Molecular Imaging* (Slart, R. H. J. A., Tio, R. A., Elsinga, P. H., and Schwaiger, M., Eds.), pp 201–234, Springer, Berlin.
- (34) Graefe, K.-H., and Bönisch, H. (1988) The transport of amines across axonal membranes of noradrenergic and dopaminergic neurones. In *Catecholamines I, Handbook of Experimental Pharmacology* (Trendelenburg, U., and Werner, N., Eds.), pp 192–245, Springer-Verlag, Berlin.
- (35) Garg, P. K., Garg, S., and Zalutsky, M. R. (1994) Synthesis and preliminary evaluation of para- and meta- ^{18}F -fluorobenzylguanidine. *Nucl. Med. Biol.* 21, 97–103.
- (36) Zhang, H., Huang, R., Pillarsetty, N., Thorek, D. L. J., Vaidyanathan, G., Serganova, I., Blasberg, R. G., and Lewis, J. S. (2014) Synthesis and evaluation of ^{18}F -labeled benzylguanidine analogs for targeting the human norepinephrine transporter. *Eur. J. Nucl. Med. Mol. Imaging* 41, 322–332.
- (37) Berry, C. R., Garg, P. K., Zalutsky, M. R., Coleman, R. E., and DeGrado, T. R. (1996) Uptake and retention kinetics of para-fluorine-18-fluorobenzylguanidine in isolated rat heart. *J. Nucl. Med.* 37, 2011–2016.
- (38) Berry, C. R., Garg, P. K., DeGrado, T. R., Hellyer, P., Weber, W., Garg, S., Hansen, B., Zalutsky, M. R., and Coleman, R. E. (1996) Para-

[^{18}F]fluorobenzylguanidine kinetics in a canine coronary artery occlusion model. *J. Nucl. Cardiol.* 3, 119–129.

(39) Jang, K. S., Jung, Y. W., Sherman, P. S., Quesada, C. A., Gu, G., and Raffel, D. M. (2013) Synthesis and bioevaluation of [^{18}F]4-fluoro-*m*-hydroxyphenethylguanidine ([^{18}F]4F-MHPG): a novel radiotracer for quantitative PET studies of cardiac sympathetic innervation. *Bioorg. Med. Chem. Lett.* 23, 1612–1616.

(40) Taegtmeier, H., Hems, R., and Krebs, H. A. (1980) Utilization of energy providing substrates in the isolated working rat heart. *Biochem. J.* 186, 701–711.

(41) Raffel, D., Loc'h, C., Mardon, K., Mazière, B., and Syrota, A. (1998) Kinetics of the norepinephrine analog [Br-76]-*meta*-bromobenzylguanidine in isolated working rat heart. *Nucl. Med. Biol.* 25, 1–16.

(42) Qi, J., and Leahy, R. M. (2000) Resolution and noise properties of MAP reconstruction for fully 3D-PET. *IEEE Trans. Med. Imaging* 19, 493–506.

(43) Narimatsu, S., Kobayashi, N., Asaoka, K., Masubuchi, Y., Horie, T., Hosokawa, M., Ishikawa, T., Ohmori, S., Kitada, M., Miyano, J., Kataoka, H., and Yamamoto, S. (2001) High-performance liquid chromatographic analysis of the sulfation of 4-hydroxypropranolol enantiomers by monkey liver cytosol. *Chirality* 13, 140–147.

(44) National Research Council (1985) *Guide for the Care and Use of Laboratory Animals*, U.S. Department of Health and Human Services, National Institutes of Health, Bethesda, MD.